Facile Synthesis of C_{60}-Nano Materials and their Application in High-Performance Water Splitting Electrocatalysis

SCHOLARONE™
Manuscripts

Facile Synthesis of C_{60}-Nano Materials and their Application in High-Performance Water Splitting Electrocatalysis

Olivia Fernandez-Delgado,[a†] Alain R. Puente-Santiago, [a†]* Manuel Cano,[b] Juan J. Giner-Casares, [b] Alejandro J. Metta-Magaña,[a] and Luis Echegoyen.*[a]

[a] Department of Chemistry and Biochemistry, University of Texas at El Paso, 500 West University Avenue, El Paso, Texas 79968, United States

[b] Departamento de Química Física y Termodinámica Aplicada, Instituto Universitario de Nanoquímica (IUNAN), Facultad de Ciencias, Universidad de Córdoba, Campus de Rabanales, Ed. Marie Curie, E-14071 Córdoba, Spain

† These authors contributed equally.

Abstract

Here, we report the synthesis and characterization of crystalline C_{60} nanomaterials and their applications as bifunctional water splitting catalysts. The shapes of the resulting materials were tuned via a solvent engineering approach to form rhombic-shaped nanosheets and nanotubes with hexagonal close packed-crystal structures. The as-synthesized materials exhibited suitable properties as bifunctional catalysts for HER and ORR reactions surpassing by far the electrocatalytic activity of commercially available amorphous C_{60}. The C_{60} nanotubes displayed the most efficient catalytic performance with a small onset potential of -0.13 V vs RHE and ultrahigh electrochemical stability properties towards the generation of molecular hydrogen. Additionally, the rotating-disk electrode measurements revealed that the oxygen reduction mechanism at the nanotubes electrochemical surfaces followed an effective four-electron pathway. The improved catalytic activity was attributed to the enhanced local electric fields at the high curvature surfaces.

Introduction

One of the best known and used allotropes of carbon is C_{60}. Since its discovery, it has attracted the attention of the scientific community and many efforts have been made to modify its properties and solubility by exohedral functionalization. [1-14] To date, fullerenes and their derivatives have been used in different applications such as molecular electronic devices and sensors,[15] photovoltaic devices,[16] biomedical applications such as antivirals,[17, 18] drug delivery,[19] imaging,[20] and photodynamic therapy,[21] among others.

On the other hand, several reports have been published about the morphology of C_{60} aggregates after crystallization using solvent engineering methods that yield new 1D and 2D nanoforms with novel properties for applications in the field of nanotechnology.[22-27] So far, their application as nanosensors[25] and transistors[24] have been published, demonstrating the versatility and applicability of these nanoforms of C_{60}.

The Hydrogen Evolution Reaction (HER) and Oxygen Reduction Reaction (ORR) are catalytic processes that have been studied extensively due to their potential impact in the development of energy storage and renewable energy conversion technologies.[28, 29] Because of the high cost of platinum, the search for new, cheaper and more efficient catalysts is an important research area. In the recent years, several reports have shown how carbon-based materials can effectively catalyze those reactions. [30-43] Unfortunately, most of the carbon-based materials also contain metals making them somewhat expensive. An alternative has been to functionalize and dope carbon-based materials with elements like sulphur, phosphorous, boron and nitrogen.[44-48] Wei *et al.* reported the fabrication of N-doped graphene/single-walled carbon nanotube (SWCNT) hybrids for HER and ORR. Their results show that the hybrids exhibit an excellent catalytic activity in the aforementioned reactions, in fact, the obtained ORR activity was much higher compared to the commercial 20 wt% Pt/C catalysts, and also exhibited better durability and resistance. [44] In 2015, Zhao *et al.* reported the preparation and utilization of surface-oxidized and electrochemically activated multi-wall carbon nanotubes (MWCNTs) as effective catalysts for Oxygen Evolution Reactions (OER).[49] Yan and co-workers did very similar work using boron as a dopant with MWCNTs for ORR.[45]

Although these previously reported metal-free carbon materials performed very well, the work required exhaustive synthetic procedures with many other reagents and materials. In this article, we focused our attention on inexpensive materials and on fast and affordable methods to obtain

new metal-free carbon-based catalysts to use in HER and ORR. The C_{60} nanomaterials were prepared following reported methods [50] and the resulting structures were characterized and tested as bifunctional catalysts, resulting in an improvement of the catalytic activity compared to the commercially available C_{60}.

Results and Discussion

Syntheses of the nanomaterials were performed following a reported procedures based on solvent engineering.[50] A saturated solution of pure C_{60} in toluene was filtered and placed in an ice bath until the temperature reached 15° C. Then, an excess of *tert*-butyl alcohol was slowly added, and the solution was allowed to rest for 15 minutes. After that time, the solutions were mixed and sonicated for 5 minutes and then placed in the refrigerator for 24 hours at a constant temperature of 15° C. In the case of the nanotubes, the temperature used was 18° C and the samples were re-dissolved after precipitation to obtain the tubular structures.
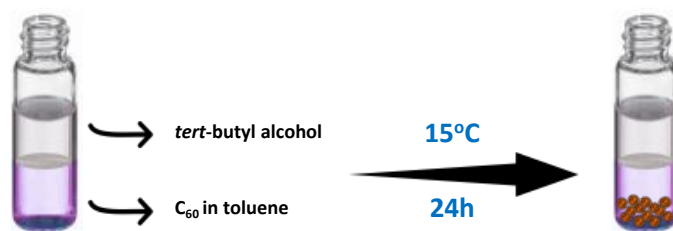

Figure 1. Scheme of the synthetic procedure of the C_{60} nanostructures

The nanomaterials obtained were filtered, dried and characterized by X-Ray Diffraction (XRD), Raman Spectroscopy, Scanning Electron Microscopy (SEM), Energy-dispersive X-ray spectroscopy (EDX) and Transmission Electron Microscopy (TEM).
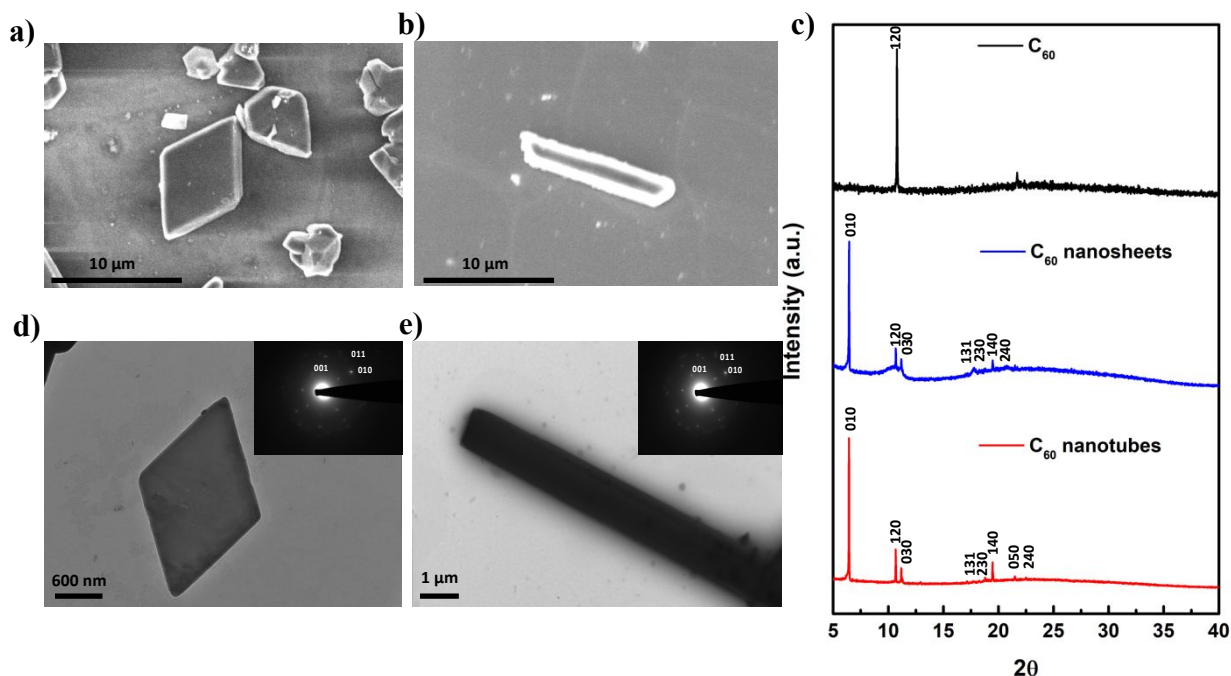
Figure 2. Characterization of the C_{60} nanostructures: SEM of a) C_{60} nanosheets and b) C_{60} nanotubes, c) XRD, and TEM of d) C_{60} nanosheets and e) C_{60} nanotubes (inset showing selective area electron diffraction patterns).

SEM of the nanostructures deposited onto silicon wafers was performed. Additionally, TEM measurements were conducted (Figure 2d and 2e). For the C_{60} nanotube samples, hollow tubes of around 10 μm were observed (Figure 2b). The sample was very homogeneous, and the size distribution of the nanotubes was very uniform (Figure S1). In the case of the C_{60} nanosheet samples, the sheets observed were not perfectly uniform in terms of shape but most of them were rhombic (Figure 2a).

EDX was performed with both structures, and for the selected areas of the nanotubes and nanosheets, only a carbon signal was observed (Figure S2). To investigate more about the packing at the molecular level, XRD measurements were conducted (Figure 2c). The samples were tested as thin films deposited on glass. Commercially available C_{60} was used as the reference, which was found to be amorphous, having a strong signal at around 10°. For the C_{60} nanotubes and nanosheets, the XRD pattern showed a hexagonal close packing (hcp) that matches with previous reports found in the literature.[22-24, 51]. Overall, the most important peaks of the hcp are present at around 4°, 11°, 11.5°, 17.8°, 18.5°, 19°, 21.7° and 22.6° that correspond to the 010, 120, 030, 131, 230, 140, 050

and 240 facets respectively. These results were further confirmed by selective area electron diffraction (SAED) measurements that clearly show a hcp in both samples (inset Figure 2d and 2e).
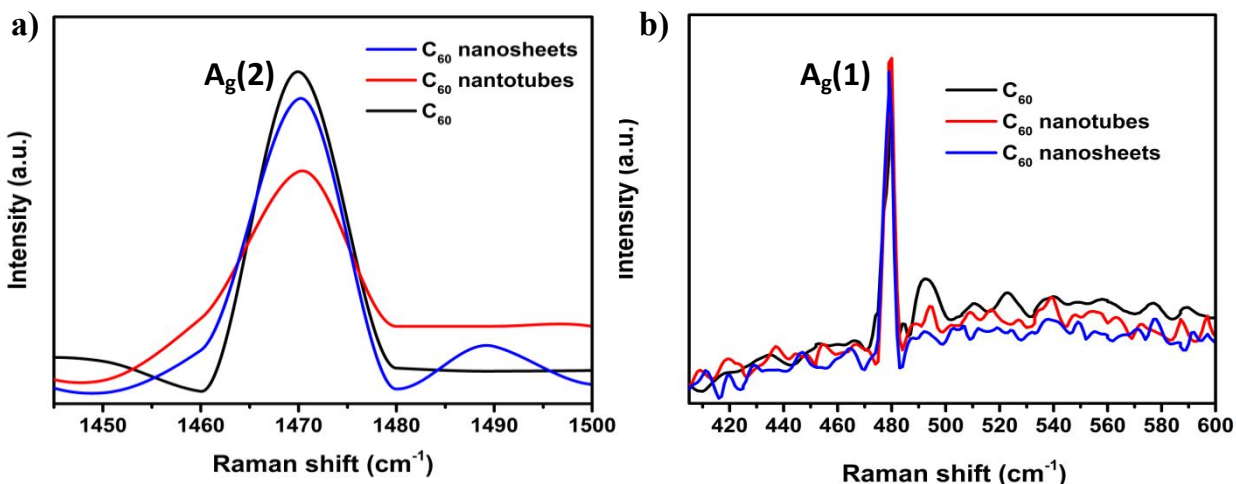

Figure 3. Raman characterization of the C_{60} nanostructures.

Raman measurements were conducted and the typical $A_g(2)$ and $A_g(1)$ bands at around 1470 and 480 cm^{-1}, respectively, were present for all samples (Figure 3a and b). It is worth to mention that no shift was observed for any of the samples when compared to amorphous C_{60}. UV-Vis characteristics were measured, and the results showed that for samples at the same concentration there were not pronounced differences of the absorption spectra (Figure S3).

HER activity of the carbon nanoforms

Electrochemical HER analysis was carefully performed for C_{60}, C_{60} nanosheets and C_{60} nanotube samples in acidic solution (0.5 M H_2SO_4 at 2 mV·s^{-1}), under static (Figure 4a) and dynamic (Figure 4c) conditions, to both assess their catalytic performance as cathode materials for water splitting and explore the effect of the dimensionality of the 0D C_{60} molecules, 1D C_{60} nanotubes, and 2D C_{60} nanosheets. This is the first time, to the best of our knowledge, that the electrocatalytic properties of differently shaped C_{60} carbon-based materials, formed from the supramolecular interactions of fullerenes molecules, are reported. Our findings revealed that C_{60} molecules exhibited the worse HER properties with a large onset potential close to -0.54 V, which can be linked to the very weak interactions between the hydrogen adsorbed species and the nanocage surfaces, that exhibit a high positive value of ΔG_H=0.44 eV.[30] On the other hand, the C_{60} nanotubes

showed very promising HER performance, exhibiting a small onset potential of -0.13 V and a Tafel slope of 84 mV · dec^{-1}, which significantly surpassed the values of -0.21 V and 340 mV·dec^{-1} obtained for the onset overpotential and the Tafel slope of the C_{60} shaped rhombic nanosheets, respectively (Figure 4a and b).
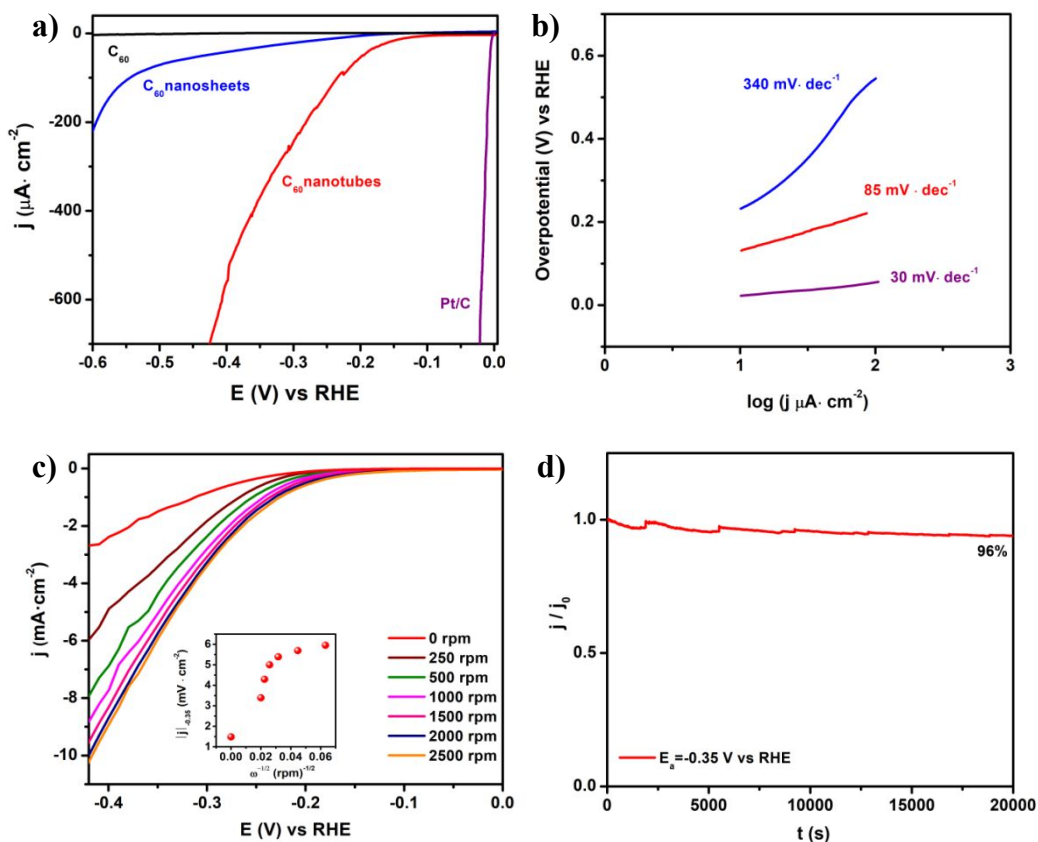

Figure 4. a) LSVs under static conditions and b) corresponding Tafel plots for HER of C_{60}, C_{60} nanosheets and C_{60} nanotubes in 0.5 M H_2SO_4 at 2 mV · s^{-1}, c) Rotating disk voltammograms (RDVs) curves at different rotation rates for the C_{60} nanotubes. Inset shows the j vs $\omega^{-1/2}$ plots, d) I-t curve of the C_{60} nanotubes at -0.35 V vs RHE.

It is worth noting that the onset overpotential for the C_{60}-nanotubes is very close to those of other state-of-the-art HER catalysts (Figure 5).
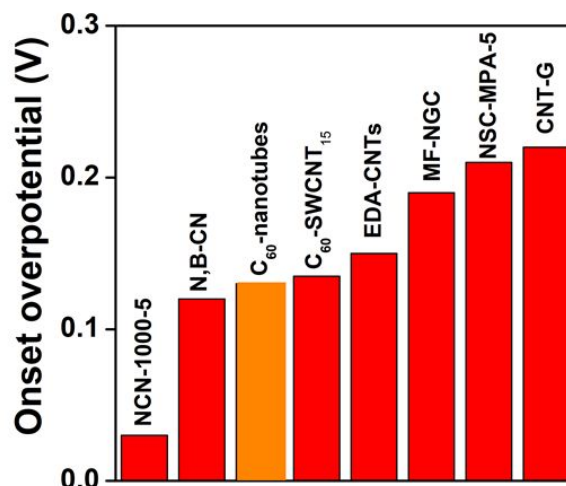
Figure 5. Comparison of the onset HER overpotential of C_{60}-nanotube electrocatalysts with other high-performance metal-free carbon-based material reported in the literature: NCN-1000-5,[52] N,B-CN,[53] C_{60}-SWCNT$_{15}$,[54] EDA-CNTs,[55] MF-NGC,[56] NSC-MPA-5[57] and CNT-G.[58]

These results indicate that the electrocatalytic efficiency for the production of hydrogen is significantly improved on the curved C_{60} nanotube surfaces. It has been recently established that the dimensionality of metal-free carbon-based electrocatalysts can strikingly change their electrocatalytic properties by tuning the mass-transport capabilities. [31] Li Song *et. al* have shown that the mass transfer of protons is improved on Pt-single atoms on nanosized onion-like carbons instead of Pt-functionalized 2D graphene materials due to the influence of very intense localized electric fields at the curved surfaces. This phenomenon, called *"tip effect"*, is able to promote an increase of reactant species at very hot active sites of the curved interfaces, which dramatically increases the electrocatalytic activity of the curved surfaces compared with the flat materials due to a decrease of the ΔG for the hydrogen adsorption processes.[32] Similarly, the improved electroreduction of CO_2 molecules at high-curvature nanostructured surfaces published by Sargent *et. al* was attributed to the action of very strong electric fields at nanoconfined spaces of the electrochemical interfaces.[33] Therefore, we propose that the electronic environment, as well as the mass transport properties, might be different for clusters of C_{60} molecules located at high-curvature areas, which could give rise to an enhanced local electric field in the aforementioned nanosurfaces and increase the proton concentrations around the active sites, facilitating the electrocatalytic HER activity. The surface area is also another important factor that can determine the catalytic activity of carbon-based water splitting electrocatalysts.[34] Obviously, the carbon nanotube supramolecular

structures possess much larger surface area values which contribute to an increase of the number of active sites and of the catalytic yields.

The HER mechanistic pathway was evaluated by rotating disk electrode measurements at different rotation rates (i.e. from 250 to 2500 r.p.m). In addition, -417 mV was the obtained potential at 10 mA·cm^{-2} and 2500 r.p.m, which is an essential parameter to know the efficiency of these type of HER electrocatalysts and, in turn, suggest an improved catalytic performance of the C_{60} nanotubes under dynamic conditions. [35, 36] Figure 4c confirmed that, for C_{60} nanotubes electrocatalysts, proton mass diffusion is the limiting step, and therefore, the Heyrovsky step may be the rate-determining step (RDS) as shown in Equation 1:[37]

$$C_{60}NT\text{-}H + H_3O^+ + e^- \leftrightarrow H_2 + H_2O + C_{60}NT \qquad \text{Eq. 1}$$
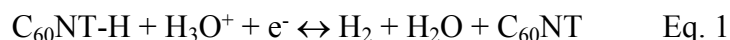
The HER durability test of the best electrocatalyst (C_{60} nanotubes) was performed by chronoamperometry at a constant potential of -350 mV vs RHE and showed high electrochemical stability (Figure 4d). To further confirm the good long-term stability, LSV curves were obtained after the durability test at 2500 r.p.m rotation rate (Figure S5). Additionally, we compared the performance of the best catalyst for HER over time. As shown in Figure S6, after 15 days the activity of the C_{60} nanotubes remained essentially the same, showing that these materials exhibit good stability over time.

ORR activity of the carbon nanoforms

The electrocatalytic performances of C_{60}, C_{60} nanosheets, and C_{60} nanotubes were successfully tested toward ORR in aqueous alkaline media (Figure 6). As shown in Figure S4, under O_2-saturated conditions the three samples exhibit very well-defined ORR cathodic peaks that are not present under Ar-saturated environments, indicating that oxygen electroreduction is taking place at the electrochemical interfaces. To gain further insights into the ORR, LSV measurements were performed at 0.5 M NaOH, 5 mV· s^{-1}. The onset ORR potentials were 0.68 V, 0. 73 V and 0.75 V for C_{60}, C_{60} nanosheets and C_{60} nanotubes, respectively. Noticeably, the positive shifts of the C_{60} onset potential when they form nanosheets and nanotubes are 150 mV and 170 mV, respectively, which clearly reveals that fullerene self-assembly is a suitable strategy to enhance the electrocatalytic activity of the individual molecules. It is important to highlight that there are not

huge differences in the catalytic behavior of C_{60} nanosheets and C_{60} nanotubes, most likely due to the lack of the tip effect on the adsorption of oxygen molecules. Therefore, the improved ORR activity of fullerenes organized into nanosheets and nanotubes could be attributed to the 3D interconnected pores which can facilitate the diffusion of the oxygen molecules to the active sites and increase the surface area and therefore the number of ORR active sites. Figure 4b and 4d show the ORR polarization curves recorded at different rotation rates and the resulting K-L plots of the C_{60} nanotube material, respectively. The excellent fittings demonstrate a first order reaction towards dissolved O_2.[46] For all the voltammograms, background currents measured under saturated Ar conditions at the same potential scan rate (5 mV·s^{-1}) were subtracted from the respective curves to eliminate the capacitive contributions. From the K-L plots and using the K-L equations, [59, 60] the average number of electrons transferred (n) per oxygen molecule at -0.1 V vs RHE was calculated (see Table 1). The number of electrons exchanged for O_2 molecules at the C_{60} nanotube electrochemical interfaces is close to 4, suggesting that the ORR reaction is following the most efficient electron pathway mechanism.

Table 1. Onset potential values (E_{on}) and average number of electrons transferred for O_2 molecule (n_e) at -0.1 V vs RHE obtained from plots in Figure 5b and 5c, respectively.

ORR Catalyst	E_{on} (V)	n_e	J_K (mA·cm^{-2})
C_{60} nanotubes	-0.125	4.390	10.41

Finally, the chronoamperometric behavior of C_{60} nanotubes in O_2-saturated at 0.7 V vs RHE were performed to unravel its long-term stability properties. The nanotubes showed an excellent electrochemical stability under basic environments, maintaining 90% of the initial current applied after 20000s.
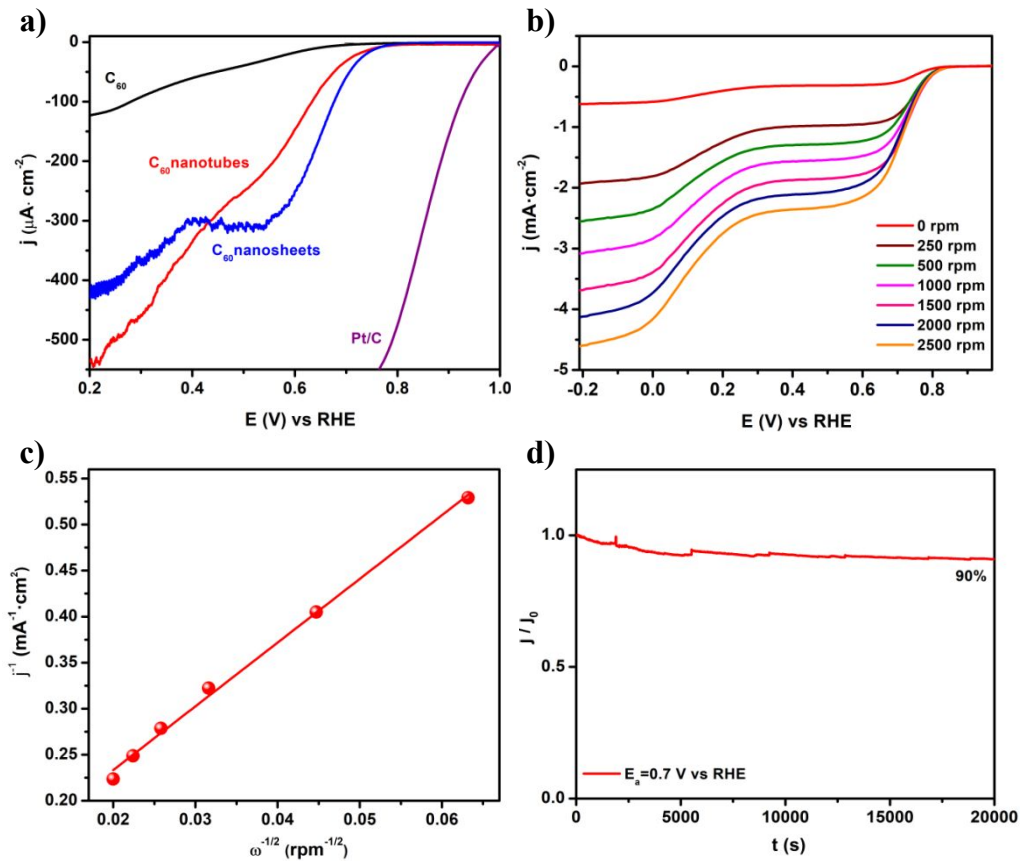
Figure 6. a) ORR polarization curves of C_{60}, C_{60} nanosheets and C_{60} nanotubes under static conditions b) RDVs at different rotation rates for the C_{60} nanotubes in 0.5 M NaOH 5 mV · s^{-1}, c) Koutecky-Levich plots obtained from Figure 4b at -0.1 V vs RHE and d) *I vs t* curve of the C_{60} nanotubes at 0.7 V vs RHE.

Materials and methods

All chemicals were reagent grade. C_{60} was purchased 99.9% from SES Research. UV Vis was performed in a Varian Cary 5000 instrument. SEM and EDX were performed in a ZEISS Sigma field-emission scanning electron microscopy, where the electron beam was accelerated in the range of 5V to 30 kV. XRD characterization was done in Panalytical Empyrean 2 using a flat sample stage and Raman measurements were taken with a Thermo Scientific DXR SmartRaman with a 532 nm lamp. TEM was performed on a H-7650 (Hitachi High Technologies, Dallas, TX) equipped with a model XR611 mid-mount digital image camera (Advanced Microscopy Techniques, Woburn, MA).

The HER and ORR performances of the carbon nanoforms were performed on an electrochemical workstation (CHI 660D) with a three-electrode system. Glassy carbon, Ag/AgCl (3M KCl) and graphite rod electrodes were used as the working, reference and counter electrodes, respectively, for both HER and ORR reactions. 0.5 M H_2SO_4 and 0.1 M NaOH solutions were used as electrolytes for the HER and ORR reactions, respectively. To make the working electrodes, 1 mg of the catalysts were dispersed in 1 mL of toluene and, subsequently, 10 μl of ink were deposited on the surface of the glassy carbon electrode. Linear sweep voltammetry (LSV) was carried out in 0.5 M H_2SO_4 solutions at 2 mV · s^{-1} and O_2-saturated 0.5 M NaOH solution at 5 mV·s^{-1} for HER and ORR reaction, respectively. Rotating disk electrode (RDE) measurements were performed using a glassy carbon (GC) disk (5 mm in diameter; A = 0.2 cm^2) electrode from Pine Instrument Co.

Conclusions

In this work, fullerene C_{60} was used as the building block to fabricate shaped-defined carbon-based electrocatalysts through a solvent engineering strategy. Rhombic-shaped 2D nanosheets and 1D nanotubes with hexagonal close-packed structures were successfully obtained. The as-synthesized C_{60} nanomaterials were tested as bifunctional catalysts for HER and ORR. The obtained results showed an enhancement of the catalytic activity of the nanomaterials when compared to the commercially available amorphous C_{60}. The best performance was observed for the C_{60} nanotubes with a very low HER onset potential of -0.13V and an excellent electrochemical stability over time, retaining 96% of the initial applied current. In addition, these materials showed a promising behavior for ORR with an onset potential of 0.73V and 0.75V for C_{60} nanosheets and C_{60} nanotubes, respectively. These values represent 0.15V and 0.17V more than the measured value for C_{60}. For the best performing material, the C_{60} nanotubes, we performed rotating disk electrode studies and the results revealed an efficient 4-electron mechanism for the ORR. The fullerene self-assembly process constituted a suitable strategy to obtain relatively inexpensive and efficient materials that can act as bifunctional metal-free catalysts.

Acknowledgements

ASOCIATED CONTENT

Supporting Information

SEM of the C_{60} nanotubes. UV-Vis and EDX characterization for C_{60} nanomaterials. Cyclic Voltammogram under Ar-saturated solutions and Oxygen-saturated solution and LSV after durability tests for C_{60} nanomaterials.

AUTHOR INFORMATION

Corresponding Author:

*Email: echegoyen@utep.edu

arpuentesan@utep.edu

Conflict of interest

No conflict of interest to declare

References

1.   P. Choubey, A. Oudhia, and R. Dewangan, *Recent Res. Sci. Technol*, 2012, **4**, 99-101.

2.   W. Kratschmer, L. D. Lamb, K. Fostiropoulos and D. R. Huffman, *Nature.*, 1990, **347**, 354-358.

3.   A. Hirsch and M. Brettreich, in *Fullerenes*, Wiley-VCH Verlag GmbH & Co. KGaA: Weinheim, Germany, 2004, pp. 383-415.

4.   A. Hirsch, *Angew. Chem. Int. Ed.*, 1993, **32**, 1138-1141.

5.   A. Hirsch, in *Fullerenes and Related Structures*, Springer Berlin Heidelberg, 1999, vol. 199, ch. 1, pp. 1-65.

6.   C. Muqing, XingLu, R. C. Maira, I. Marta and E. Luis, in *Endohedral Metallofullerenes*, CRC Press, 2014.

7.   C. Thilgen, A. Herrmann and F. Diederich, *Angew. Chem. Int. Ed.*, 1997, **36**, 2268-2280.

8.   N. Martin, *Chem. Commun.*, 2006, 2093-2104.

9.   A. Hirsch and M. Brettreich, in *Fullerenes*, Wiley-VCH Verlag GmbH & Co. KGaA, 2005, pp. 1-48.

10.   H. W. Kroto, J. R. Heath, S. C. O'Brien, R. F. Curl and R. E. Smalley, *Nature.*, 1985, **318**, 162-163.

11.   E. Castro, J. Murillo, O. Fernandez-Delgado and L. Echegoyen, *J. Mater. Chem. C.*, 2018, **6**, 2635-2651.

12.   L.-L. Deng, S.-Y. Xie and F. Gao, *Adv. Electron. Mater.* , 2017, 1700435.

13.   L. Pasimeni, A. Hirsch, I. Lamparth, A. Herzog, M. Maggini, M. Prato, C. Corvaja and G. Scorrano, *J. Am. Chem. Soc.*, 1997, **119**, 12896-12901.

14.   P. W. Fowler, *J. Chem. Soc., Faraday Trans.*, 1995, **91**, 2241-2247.

15.   C. A. Martin, D. Ding, J. K. Sorensen, T. Bjornholm, J. M. van Ruitenbeek and H. S. van der Zant, *J. Am. Chem. Soc.*, 2008, **130**, 13198-13199.

16.   C.-Z. Li, H.-L. Yip and A. K. Y. Jen, *J. Mater. Chem.*, 2012, **22**, 4161-4177.

17.   S. H. Friedman, D. L. DeCamp, R. P. Sijbesma, G. Srdanov, F. Wudl and G. L. Kenyon, *J. Am. Chem. Soc.*, 1993, **115**, 6506-6509.

18.   E. A. Khakina, O. g. A. Kraevaya, M. L. Popova, A. S. Peregudov, S. I. Troyanov, A. V. Chernyak, V. M. Martynenko, A. V. Kulikov, D. Schols and P. A. Troshin, *Org. Biomol. Chem.*, 2016, 15, 773-777 .

19.   A. Montellano, T. Da Ros, A. Bianco and M. Prato, *Journal*, 2011, **3**, 4035-4041.

20.   Z. Chen, L. Ma, Y. Liu and C. Chen, *Theranostics.*, 2012, **2**, 238-250.

21.   P. Mroz, G. P. Tegos, H. Gali, T. Wharton, T. Sarna and M. R. Hamblin, *Photochem. Photobiol. Sci.*, 2007, **6**, 1139-1149.

22.   M. Yao, B. M. Andersson, P. Stenmark, B. Sundqvist, B. Liu and T. Wågberg, *Carbon*, 2009, **47**, 1181-1188.

23.   R. Colle, G. Grosso, A. Ronzani, M. Gazzano and V. Palermo, *Carbon*, 2012, **50**, 1332-1337.

24.   C. Larsen, H. R. Barzegar, F. Nitze, T. Wågberg and L. Edman, *Nanotechnology*, 2012, **23**, 344015.

25.   J. A. Rather, A. J. Al Harthi, E. A. Khudaish, A. Qurashi, A. Munam and P. Kannan, *Anal. Methods*, 2016, **8**, 5690-5700.

26.   M. Sathish and K. i. Miyazawa, *J. Am. Chem. Soc.*, 2007, **129**, 13816-13817.

27.   J. D. Fortner, D. Y. Lyon, C. M. Sayes, A. M. Boyd, J. C. Falkner, E. M. Hotze, L. B. Alemany, Y. J. Tao, W. Guo, K. D. Ausman, V. L. Colvin and J. B. Hughes, *Environ. Sci. Technology*, 2005, **39**, 4307-4316.

28.   G.-G. Luo, H.-L. Zhang, Y.-W. Tao, Q.-Y. Wu, D. Tian and Q. Zhang, *Inorg. Chem. Front.*, 2019, **6**, 343-354.

29.   D.-D. Huang, S. Li, Y.-P. Wu, J.-H. Wei, J.-W. Yi, H.-M. Ma, Q.-C. Zhang, Y.-L. Liu and D.-S. Li, *Chem. Comm.*, 2019, **55**, 4570-4573.

30.   T. He, G. Gao, L. Kou, G. Will and A. Du, *J. Catal.*, 2017, **354**, 231-235.

31.   L. Yang, J. Shui, L. Du, Y. Shao, J. Liu, L. Dai and Z. Hu, *Adv. Mater.*, 2019, **31**, 1804799.

32.   D. Liu, X. Li, S. Chen, H. Yan, C. Wang, C. Wu, Y. A. Haleem, S. Duan, J. Lu, B. Ge, P. M. Ajayan, Y. Luo, J. Jiang and L. Song, *Nat. Energy*, 2019, **4**, 512-518.

33.   M. Liu, Y. Pang, B. Zhang, P. De Luna, O. Voznyy, J. Xu, X. Zheng, C. T. Dinh, F. Fan, C. Cao, F. P. G. de Arquer, T. S. Safaei, A. Mepham, A. Klinkova, E. Kumacheva, T. Filleter, D. Sinton, S. O. Kelley and E. H. Sargent, *Nature*, 2016, **537**, 382-386.

34.   L. Zhang, J. Xiao, H. Wang and M. Shao, *ACS Catalysis*, 2017, **7**, 7855-7865.

35. D. Alba-Molina, A. R. Puente Santiago, J. J. Giner-Casares, E. Rodríguez-Castellón, M. T. Martín-Romero, L. Camacho, R. Luque and M. Cano, *J. Mater. Chem. A*, 2019, **7**, 20425-20434.

36. D. Rodríguez-Padrón, A. R. Puente-Santiago, M. Cano, A. Caballero, M. J. Muñoz-Batista and R. Luque, *ACS Appl. Mater. Interfaces*, 2020, **12**, 2207-2215.

37. C. Costentin, M. Robert and J.-M. Savéant, *Chem. Rev*, 2010, **110**, PR1-PR40.

38. X. Wang, A. Vasileff, Y. Jiao, Y. Zheng and S.-Z. Qiao, *Adv. Mater.*, 2019, **31**, 1803625.

39. R. Paul, L. Zhu, H. Chen, J. Qu and L. Dai, *Adv. Mater.*, 2019, **31**, 1806403.

40. L. Tao, Y. Wang, Y. Zou, N. Zhang, Y. Zhang, Y. Wu, Y. Wang, R. Chen and S. Wang, *Adv. Energy Mater.*, **n/a**, 1901227.

41. L. Dai, *Curr. Opin. Electrochem.*, 2017, **4**, 18-25.

42. T. He, G. Gao, L. Kou, G. Will and A. Du, *J. Catal.*, 2017, **354**, 231-235.

43. M. Chen, R. Guan and S. Yang, *Adv. Sci.*, 2019, **6**, 1800941.

44. G.-L. Tian, M.-Q. Zhao, D. Yu, X.-Y. Kong, J.-Q. Huang, Q. Zhang and F. Wei, *Small*, 2014, **10**, 2251-2259.

45. Y. Cheng, Y. Tian, X. Fan, J. Liu and C. Yan, *Electrochim. Acta*, 2014, **143**, 291-296.

46. G. Tuci, C. Zafferoni, A. Rossin, A. Milella, L. Luconi, M. Innocenti, L. Truong Phuoc, C. Duong-Viet, C. Pham-Huu and G. Giambastiani, *Chem. Mater*, 2014, **26**, 3460-3470.

47. J. P. Paraknowitsch and A. Thomas, *Energ. Environ. Sci.*, 2013, **6**, 2839-2855.

48. N. Daems, X. Sheng, I. F. J. Vankelecom and P. P. Pescarmona, *J. Mater. Chem. A*, 2014, **2**, 4085-4110.

49. X. Lu, W.-L. Yim, B. H. R. Suryanto and C. Zhao, *J. Am. Chem. Soc.*, 2015, **137**, 2901-2907.

50. M. Sathish, K. i. Miyazawa, J. P. Hill and K. Ariga, *J. Am. Chem. Soc.*, 2009, **131**, 6372-6373.

51. J. A. Rather, A. J. Al Harthi, E. A. Khudaish, A. Qurashi, A. Munam and P. Kannan, *Anal. Methods*, 2016, **8**, 5690-5700.

52. H. Jiang, J. Gu, X. Zheng, M. Liu, X. Qiu, L. Wang, W. Li, Z. Chen, X. Ji and J. Li, *Energy Environ. Sci.*, 2019, **12**, 322-333.

53. K. Qu, Y. Zheng, X. Zhang, K. Davey, S. Dai and S. Z. Qiao, *ACS Nano*, 2017, **11**, 7293-7300.

54. R. Gao, Q. Dai, F. Du, D. Yan and L. Dai, *J. Am. Chem. Soc.*, 2019, **141**, 11658-11666.

55. T. Li, D. Tang, Z. Cui, B. Cai, D. Li, Q. Chen and C. Li, *Electrocatalysis*, 2018, **9**, 573-581.

56. P. Thirukumaran, R. Balasubramanian, R. Atchudan, A. Shakila Parveen, Y. R. Lee and S.-C. Kim, *Mater. Res. Bull.*, 2020, **124**, 110734.

57. A. Mulyadi, Z. Zhang, M. Dutzer, W. Liu and Y. Deng, *Nano Energy*, 2017, **32**, 336-346.

58. T. Odedairo, X. Yan, G. Gao, X. Yao, A. Du and Z. Zhu, *Carbon*, 2016, **107**, 739-746.

59. S. Guo, S. Zhang, L. Wu and S. Sun, *Angew. Chem*, 2012, **51**, 11770-11773.

60. A. Franco, M. Cano, J. J. Giner-Casares, E. Rodríguez-Castellón, R. Luque and A. R. Puente-Santiago, *Chem. Comm*, 2019, **55**, 4671-4674.

Table of content (TOC)